Double ionization of helium by fast electrons with the Generalized Sturmian Functions method

2015 J. Phys. B: At. Mol. Opt. Phys. 48 055204

(http://iopscience.iop.org/0953-4075/48/5/055204)

IOP Publishing Journal of Physics B: Atomic, Molecular and Optical Physics
J. Phys. B: At. Mol. Opt. Phys. **48** (2015) 055204 (13pp) doi:10.1088/0953-4075/48/5/055204

Double ionization of helium by fast electrons with the Generalized Sturmian Functions method

M J Ambrosio[1,6], F D Colavecchia[2,6], G Gasaneo[3,6], D M Mitnik[1,4,6] and L U Ancarani[5]

[1] Instituto de Astronomía y Física del Espacio (IAFE, CONICET–UBA), Buenos Aires, Argentina
[2] División Física Atómica, Molecular y Óptica, Centro Atómico Bariloche, 8400 S. C. de Bariloche, Río Negro, Argentina
[3] Departamento de Física, Universidad Nacional del Sur, 8000 Bahía Blanca, Buenos Aires, Argentina
[4] FCEyN Universidad de Buenos Aires, Argentina
[5] Théorie, Modélisation, Simulation, SRSMC, UMR CNRS 7565, Université de Lorraine, 57078 Metz, France
[6] Consejo Nacional de Investigaciones Científicas y Técnicas, CONICET, Argentina

E-mail: mja1984@gmail.com

Received 15 October 2014, revised 7 January 2015
Accepted for publication 19 January 2015
Published 11 February 2015

Abstract

The double ionization of helium by high energy electron impact is studied. The corresponding four-body Schrödinger equation is transformed into a set of driven equations containing successive orders in the projectile–target interaction. The first order driven equation is solved with a generalized Sturmian functions approach. The transition amplitude, extracted from the asymptotic limit of the first order solution, is equivalent to the familiar first Born approximation. Fivefold differential cross sections are calculated for (e, 3e) processes within the high incident energy and small momentum transfer regimes. The results are compared with other numerical methods, and with the only absolute experimental data available. Our cross sections agree in shape and magnitude with those of the convergent close coupling method for the (10+10) eV and (4+4) eV emission energies. To date this had not been achieved by any two different numerical schemes when solving the three–body continuum problem for the fast projectile (e, 3e) process. Though agreement with the experimental data, in particular with respect to the magnitude, is not achieved, our findings partly clarify a long standing puzzle.

Keywords: helium, double ionization, first born, fully differential cross section

(Some figures may appear in colour only in the online journal)

1. Introduction

The understanding of the quantum dynamics of few-body problems is a matter of considerable importance. On one side, from its fundamental point of view, and, on the other, from the point of view of the applications it may have (see, e.g., [1–3]). It has been said in the literature that the three-body quantum mechanical scattering problem has been numerically solved, proofs being given by the study of the hydrogen ionization by electron impact [4, 5] and the double photo–ionization of helium [6–8]. Time-independent methods such as the exterior complex scaling, the convergent close coupling (CCC) and the J-matrix have been able to successfully describe the aforementioned processes (see the review paper [9]). A serious challenge to this affirmation comes from the analysis of the double ionization of Helium by high energy electron impact. For high projectile energies, this four-body scattering process can be reduced to a three-body one [10]. In [11] it was shown that the first Born approximation for the transition amplitude is equivalent to solving a driven equation satisfied by the scattering part of the wave function, the latter describing the dynamics of the ionization process. As

discussed in [12] (and in the introduction of [11] with updated references), the J-Matrix [13–15], CCC [16] and wavepacket evolution [17] methods have been applied to the description of the $(e, 3e)$ (electron impact double ionization) process on helium, and no agreement is found between them. On top of that, none of them globally agrees with the absolute experimental data [16, 18]. The fact that three *ab initio* methods do not agree is quite remarkable, since they are solving essentially the same mathematical problem. We wonder why this occurs and that encourages us to study this problem carefully.

In this contribution, we continue with the studies initiated in [11] and [19] by obtaining and analyzing the full solution to the three-body scattering problem that results from the high energy $(e, 3e)$ process on helium. The generalized Sturmian functions (GSF) approach [20] is used to numerically evaluate the solution. From it, fully differential cross sections are extracted, and compared with those obtained experimentally and by other theoretical methods, in particular the CCC and J-Matrix.

In a previous publication [11] we transformed the four-body Schrödinger equation into a system of coupled non-homogeneous equations where the left-hand-side includes a simplified Hamiltonian including the three-body helium interactions plus a free particle (projectile) kinetic term. All the interactions (coupling) between the projectile and the helium target were included in the driven term of each of the system equations. In [11] we formulated the general problem, but we provided GSF results only for a *S*-wave model. In [21], we presented preliminary results for scattering solutions with non-zero angular momenta, demonstrating the numerical convergence of the GSF approach; only single differential cross sections were shown. In this contribution we continue with these investigations. We present GSF calculations for the full three-body solution describing the $(e, 3e)$ process on helium by impact of high energy electrons. Details on the wave function construction are provided. In addition, and with the aim of testing the procedure, we deliberately extract the ionization amplitude—and thus the cross sections—from the scattering wave function itself. This is possible because, as we will show, the solution of the driven equation builds the correct hyperspherical wave front not only for the S-wave, as shown in previous publications, but also for all other partial waves.

The paper is organized as follows. In section 2 we present the theory on which our fast-projectile formulation of the problem is based upon. Formulae and details of how the resulting equation is solved, and how the collision information is extracted, are provided in section 3. Section 4 presents the results obtained with the GSF method for both kinematic conditions considered in the Orsay experiment of 1999 [16, 18], namely, (10+10) eV and (4+4) eV emission energies; for several geometries qualitative and quantitative comparison is made with the J-Matrix and CCC results.

Atomic units ($\hbar = e = m_e = 1$) are assumed throughout, unless stated otherwise.

2. General theory

The Hamiltonian for three electrons and an infinite mass helium nucleus of charge $Z = 2$ is given by

$$H = -\frac{1}{2}\nabla_1^2 - \frac{1}{2}\nabla_2^2 - \frac{1}{2}\nabla_3^2 - \frac{Z}{r_1} - \frac{Z}{r_2} - \frac{Z}{r_3} + \frac{1}{r_{12}} + \frac{1}{r_{13}} + \frac{1}{r_{23}}, \tag{1}$$

where particle 1 labels the electron projectile, while particles 2 and 3 are the target electrons. We also define the operators

$$h_{\rm He} = \left(-\frac{1}{2}\nabla_2^2 - \frac{1}{2}\nabla_3^2 - \frac{Z}{r_2} - \frac{Z}{r_3} + \frac{1}{r_{23}}\right), \tag{2a}$$

$$h_p = -\frac{1}{2}\nabla_1^2, \tag{2b}$$

where $h_{\rm He}$ is the three-body helium Hamiltonian (subsystem (2, 3)), while h_p is the free-particle kinetic term associated to the projectile (subsystem 1). With these definitions, we decompose the four-body Hamiltonian as follows:

$$H = H_0 + \bar{W}. \tag{3}$$

where

$$H_0 = h_p + h_{\rm He}, \tag{4a}$$

$$\bar{W} = -\frac{Z}{r_1} + \frac{1}{r_{12}} + \frac{1}{r_{13}}. \tag{4b}$$

The Hamiltonian H_0 includes all the interactions of the subsystem (2, 3) through $h_{\rm He}$. The two subsystems are coupled through the interaction $\bar{W}$.

For a four-body problem as the $(e, 3e)$ process we need to find a scattering solution, with outgoing (+) type-behavior, of the four-body Schödinger equation

$$\left[H_0 + \bar{W} - E\right]\Psi^+(\mathbf{r}_1, \mathbf{r}_2, \mathbf{r}_3) = 0, \tag{5}$$

where E is the total energy. As shown in [11], the Schödinger equation (5) can be transformed into a system of coupled differential equations if the solution is proposed as:

$$\Psi^+(\mathbf{r}_1, \mathbf{r}_2, \mathbf{r}_3) = \sum_n \Psi^{(n)+}(\mathbf{r}_1, \mathbf{r}_2, \mathbf{r}_3), \tag{6}$$

where each order contains n interactions $\bar{W}$ between the projectile and the target. In particular, the equations corresponding to the zero and first order read:

$$\left[H_0 - E\right]\Psi^{(0)+}(\mathbf{r}_1, \mathbf{r}_2, \mathbf{r}_3) = 0, \tag{7a}$$

$$\left[H_0 - E\right]\Psi^{(1)+}(\mathbf{r}_1, \mathbf{r}_2, \mathbf{r}_3) = -\bar{W}\Psi^{(0)+}(\mathbf{r}_1, \mathbf{r}_2, \mathbf{r}_3), \tag{7b}$$

Clearly, the solution corresponding to the zeroth-order equation (7*a*), $\Psi^{(0)+}(\mathbf{r}_1, \mathbf{r}_2, \mathbf{r}_3)$, is separable in the two particle subsystems (2, 3) and 1 (see equation (4a)) and reads

$$\Psi^{(0)+}(\mathbf{r}_1, \mathbf{r}_2, \mathbf{r}_3) = \frac{1}{(2\pi)^{3/2}} e^{i\mathbf{k}_i\cdot\mathbf{r}_1}\Phi_i(\mathbf{r}_2, \mathbf{r}_3). \tag{8}$$

Here $\Phi_i(\mathbf{r}_2, \mathbf{r}_3)$ represents the ground state of the helium

atom; the incident projectile is represented by a plane wave of momentum $\mathbf{k}_i$.

The first order solution, which satisfies equation (7*b*), can be written as [11]:

$$\Psi^{(1)+}(\mathbf{r}_1, \mathbf{r}_2, \mathbf{r}_3) = \frac{1}{(2\pi)^{3/2}} \int \mathrm{d}\mathbf{k}\, \mathrm{e}^{\mathrm{i}\mathbf{k}\cdot\mathbf{r}_1}\, \Phi^{+}_{sc}(\mathbf{k}, \mathbf{r}_2, \mathbf{r}_3), \quad (9)$$

where the label *sc* stands for scattering. Let E_a be the energy of two electrons in interaction with the nucleus in the final state, and $k^2/2$ the energy associated to the projectile: the total energy of the system is then $E = k^2/2 + E_a$. Replacing the proposal (9) in equation (7*b*), and taking into account that $h_p \mathrm{e}^{\mathrm{i}\mathbf{k}\cdot\mathbf{r}_1} = (k^2/2)\mathrm{e}^{\mathrm{i}\mathbf{k}\cdot\mathbf{r}_1}$, we have

$$\frac{1}{(2\pi)^{3/2}} \int \mathrm{d}\mathbf{k}\, \mathrm{e}^{\mathrm{i}\mathbf{k}\cdot\mathbf{r}_1} \left[h_{\mathrm{He}} - E_a\right] \Phi^{+}_{sc}(\mathbf{k}, \mathbf{r}_2, \mathbf{r}_3) = -\bar{W} \frac{1}{(2\pi)^{3/2}} \mathrm{e}^{\mathrm{i}\mathbf{k}_i\cdot\mathbf{r}_1} \Phi_i(\mathbf{r}_2, \mathbf{r}_3), \quad (10)$$

where the integration limits are restricted by energy conservation. Projecting by the left with a plane wave $\frac{1}{(2\pi)^{3/2}}\mathrm{e}^{\mathrm{i}\mathbf{k}_f\cdot\mathbf{r}_1}$ with momentum $\mathbf{k}_f$, i.e., selecting $\mathbf{k} = \mathbf{k}_f$ as the momentum of the scattered projectile in the final channel, we find

$$\left[h_{\mathrm{He}} - E_a\right] \Phi^{+}_{sc}(\mathbf{q}, \mathbf{r}_2, \mathbf{r}_3) = -\frac{4\pi}{q^2} \frac{1}{(2\pi)^3} \left(-Z + \mathrm{e}^{\mathrm{i}\mathbf{q}\cdot\mathbf{r}_2} + \mathrm{e}^{\mathrm{i}\mathbf{q}\cdot\mathbf{r}_3}\right) \Phi_i(\mathbf{r}_2, \mathbf{r}_3), \quad (11)$$

where $\mathbf{q} = \mathbf{k}_i - \mathbf{k}_f$ is the momentum transfer vector. As we can see from this equation, the four-body problem was reduced to a pure three-body one describing the dynamics of the two ejected electrons in the presence of the heavy nucleus. The driven equation (11) has been presented only in [11, 19].

We showed in [11] that the formal solution

$$\Phi^{+}_{sc}(\mathbf{q}, \mathbf{r}_2, \mathbf{r}_3) = \int \mathrm{d}\mathbf{r}'_2 \mathrm{d}\mathbf{r}'_3\, G^{+}_{a}\left(\mathbf{r}_2, \mathbf{r}_3, \mathbf{r}'_2, \mathbf{r}'_3\right) \times W_{fi}\left(\mathbf{r}'_2, \mathbf{r}'_3\right) \Phi_i\left(\mathbf{r}'_2, \mathbf{r}'_3\right), \quad (12)$$

of equation (11) leads to the first Born approximation for the transition amplitude. We use here $W_{fi}(\mathbf{r}_2, \mathbf{r}_3) = \frac{4\pi}{q^2}\frac{1}{(2\pi)^3}\left(-Z + \mathrm{e}^{\mathrm{i}\mathbf{q}\cdot\mathbf{r}_2} + \mathrm{e}^{\mathrm{i}\mathbf{q}\cdot\mathbf{r}_3}\right)$ and take the three-body Coulomb Green function $G^{+}_{a}\left(\mathbf{r}_2, \mathbf{r}_3, \mathbf{r}'_2, \mathbf{r}'_3\right)$ whose behaviour in the Ω_0 region reads

$$G^{+}_{a}\left(\mathbf{r}_2, \mathbf{r}_3, \mathbf{r}'_2, \mathbf{r}'_3\right) \to (2\pi\mathrm{i})^{1/2} \kappa^{\frac{3}{2}} \frac{\mathrm{e}^{\mathrm{i}\left[\kappa\rho - \lambda_0 \ln(2\kappa\rho) - \sigma_0\right]}}{\rho^{\frac{5}{2}}} \Psi^{-}_{\tilde{\mathbf{k}}_2, \tilde{\mathbf{k}}_3}\left(\mathbf{r}'_2, \mathbf{r}'_3\right), \quad (13)$$

where $\rho = (r_2^2 + r_3^2)^{1/2}$ is the hyperradius, $\kappa = (2E)^{1/2}$, σ_0 is a Coulomb phase, and λ_0 is a Sommerfeld parameter [22]; $\tilde{\mathbf{k}}_j = \frac{\kappa}{\rho}\mathbf{r}_j$ ($j = 2, 3$) are the coordinate-dependent momenta defined originally in [23] and more explicitly in [22]. The function $\Psi^{-}_{\tilde{\mathbf{k}}_2, \tilde{\mathbf{k}}_3}(\mathbf{r}_2, \mathbf{r}_3)$ is an asymptotic continuum solution accounting for the interactions of the target electrons with their parent helium nucleus. In equation (13) we modified the definition given by Kadyrov and co-workers to be in accordance with the normalization we used for the plane wave incident-scattered electron. Replacing now (13) into (12) we obtain the following asymptotic behaviour

$$\Phi^{+}_{sc}(\mathbf{q}, \mathbf{r}_2, \mathbf{r}_3) \underset{\rho\to\infty}{\longrightarrow} (2\pi\mathrm{i})^{1/2} \kappa^{\frac{3}{2}} T_{\tilde{\mathbf{k}}_2, \tilde{\mathbf{k}}_3} \frac{\mathrm{e}^{\mathrm{i}\left[\kappa\rho - \lambda_0 \ln(2\kappa\rho) - \sigma_0\right]}}{\rho^{\frac{5}{2}}}. \quad (14)$$

The transition amplitude $T_{\tilde{\mathbf{k}}_2, \tilde{\mathbf{k}}_3}$ can also be written as:

$$T_{\tilde{\mathbf{k}}_2, \tilde{\mathbf{k}}_3} = \frac{4\pi}{q^2} \frac{1}{(2\pi)^3} \left\langle \Psi^{-}_{\tilde{\mathbf{k}}_2, \tilde{\mathbf{k}}_3}(\mathbf{r}_2, \mathbf{r}_3) \right| - Z + \mathrm{e}^{\mathrm{i}\mathbf{q}\cdot\mathbf{r}_2} + \mathrm{e}^{\mathrm{i}\mathbf{q}\cdot\mathbf{r}_3} \left| \Phi_i(\mathbf{r}_2, \mathbf{r}_3) \right\rangle. \quad (15)$$

An important observation is to be made regarding the T-matrix. While the analysis of its magnitude with varying ejection momenta $\mathbf{k}_2$, $\mathbf{k}_3$, presented in [10, 18, 24] is performed directly through the matrix expression (15), in our work the same information is extracted directly from the wave function, i.e., from equation (14): the same operator $\left(-Z + \mathrm{e}^{\mathrm{i}\mathbf{q}\cdot\mathbf{r}_2} + \mathrm{e}^{\mathrm{i}\mathbf{q}\cdot\mathbf{r}_3}\right)$ appearing in equation (15) participates on the right-hand-side (RHS) of equation (11). Consequently, a particular emission geometry is directly stimulated or suppressed in our wave function via the RHS, and the kinematical analysis of [10, 18, 24] applies similarly in our formulation too.

3. The driven equation and the GSF methodology

The driven term of equation (11) regulates the behavior of the three-body scattering wave function $\Phi^{+}_{sc}(\mathbf{q}, \mathbf{r}_2, \mathbf{r}_3)$ mainly at short distances because of the limited range of the bound state $\Phi_i(\mathbf{r}_2, \mathbf{r}_3)$. We use the generalized Sturmian functions (GSF) methodology (see review [20]) to calculate both functions appearing in (11). Non-correlated, three-body basis sets are constructed as products of two-body GSF. These ones satisfy the following homogeneous second-order differential equation:

$$\left[-\frac{1}{2}\frac{\mathrm{d}^2}{\mathrm{d}r^2} + \frac{l(l+1)}{2r^2} + \mathcal{U}(r) - E_s\right] S_{nl}(r) = -\beta_{nl} \mathcal{V}(r) S_{nl}(r), \quad (16)$$

where the basis energy E_s is an externally fixed parameter and β_{nl} the eigenvalues for a given angular momentum l. The r-dependent functions $\mathcal{U}(r)$ and $\mathcal{V}(r)$ are respectively called auxiliary and generating potentials. The former has the purpose of incorporating the physics of the specific problem into the basis set. The latter, $\mathcal{V}(r)$, shapes the basis set localizing its oscillations in any region of interest, and is usually of short range to ensure all elements possess the same asymptotic behaviour dictated by $\mathcal{U}(r)$ and E_s. With a positive energy E_s one obtains GSF sets suitable for describing systems encompassing the continuum, while a negative choice of E_s generates a basis with decaying exponential behaviour, suited for bound systems. For both, the $\Phi^{+}_{sc}(\mathbf{q}, \mathbf{r}_2, \mathbf{r}_3)$ and $\Phi_i(\mathbf{r}_2, \mathbf{r}_3)$ calculations, we choose auxiliary potentials equal to the helium two-body Coulomb interaction $-\frac{Z}{r}$, in order to remove two terms in the four-body Hamiltonian. On the other hand, GSF asymptotic conditions and generating potentials are

chosen differenty for $\Phi_{sc}^{+}(\mathbf{q}, \mathbf{r}_2, \mathbf{r}_3)$ and $\Phi_i(\mathbf{r}_2, \mathbf{r}_3)$, as will be clear in the next paragraphs. For details on the numerical basis generation we refer the reader to [20, 25] and references therein.

We describe the helium ground state appearing in the RHS of equation (11) through an expansion in terms of bound type GSF:

$$\Phi_i(\mathbf{r}_2, \mathbf{r}_3) = \sum_{l_2,l_3} \sum_{n_2,n_3} \phi_\nu^{(b,b)} \Theta_\nu^{(b,b)}(\mathbf{r}_2, \mathbf{r}_3), \tag{17}$$

where the three–body basis elements $\Theta_\nu^{(b,b)}(\mathbf{r}_2, \mathbf{r}_3)$ are constructed as follows:

$$\Theta_\nu^{(b,b)}(\mathbf{r}_2, \mathbf{r}_3) = \mathcal{Y}_{l_2 l_3}^{LM}\left(\hat{\mathbf{r}}_2, \hat{\mathbf{r}}_3\right) \frac{S_{n_2 l_2}^{(b)}(r_2)}{r_2} \frac{S_{n_3 l_3}^{(b)}(r_3)}{r_3}. \tag{18}$$

For compactness, we use the ν index to denote the whole set of indices $\{L, M, l_2, l_3, n_2, n_3\}$. Note that the helium ground state corresponds to the case $L = M = 0$. Label (b) denotes the bound character of the basis, and labels 2 and 3 refer to the two target electrons. In this work the generating potential for the $S_{n_2 l_2}^{(b)}(r_2)$ and $S_{n_3 l_3}^{(b)}(r_3)$ sets is taken as a Yukawa type, in the same spirit as in previous bound states studies [20]. We include partial waves up to $l_2 = l_3 = 2$ and $l_2 = l_3 = 4$, giving energies of −2.90277 a.u. and −2.903343 a.u.; we deemed this to be sufficient as we have noticed that the addition of two partial waves did not affect importantly the calculated ionization cross sections. As will be presented in section 4, surprising results appear when using a much simplified description of the target bound state: only for this specific purpose we have also considered a GSF construction of a Temkin–Poet model of helium with a binding energy of −2.8790 a.u.

For the scattering solution, also proposed as an expansion in GSF set, the outgoing type behavior at large values of the coordinates r_2 and r_3 is enforced via the basis:

$$\Phi_{sc}^{+}(\mathbf{q}, \mathbf{r}_2, \mathbf{r}_3) = \sum_{L',M'} \sum_{l_2',l_3'} \sum_{n_2',n_3'} \phi_{\nu'}^{(c,c)} \Theta_{\nu'}^{(c,c)}(\mathbf{r}_2, \mathbf{r}_3), \tag{19}$$

with

$$\Theta_{\nu'}^{(c,c)}(\mathbf{r}_2, \mathbf{r}_3) = \mathcal{Y}_{l_2' l_3'}^{LM}\left(\hat{\mathbf{r}}_2, \hat{\mathbf{r}}_3\right) \frac{S_{n_2' l_2'}^{(c)}(r_2)}{r_2} \frac{S_{n_3' l_3'}^{(c)}(r_3)}{r_3}. \tag{20}$$

The index ν' denotes $\{L', M', l_2', l_3', n_2', n_3'\}$, and the (c) label denotes the continuum. The $S_{n_2' l_2'}^{(c)}(r_2)$ and $S_{n_3' l_3'}^{(c)}(r_3)$ are two–body GSF with outgoing behavior at large distances obtained from equation (16) using a square well type generating potential $\mathcal{V}^{(c)}(r)$, and their energy $E_s^{(c)}$ is fixed to match the total available for the two emitted electrons, E_a (see [19]).

A projection onto every basis element (20) transforms differential equation (11) into algebraic linear systems for the coefficients $\phi_\nu^{(c,c)}$, which are neatly put together as the elements of a vector $\boldsymbol{\phi}^{(c,c)}$:

$$\left[\mathbf{H} - \left(E_a - 2E_s^{(c)}\right)\mathbf{S}\right]\boldsymbol{\phi}^{(c,c)} = \boldsymbol{\varphi}. \tag{21}$$

Vector $\boldsymbol{\varphi}$ consists of the projection of the RHS of (11) onto each continuum basis element (see equation (20)). Its components, $\boldsymbol{\varphi}_{\nu''}$, are given by:

$$\boldsymbol{\varphi}_{\nu''} = \int \mathrm{d}\mathbf{r}_2 \mathrm{d}\mathbf{r}_3\, \Theta_{\nu''}^{(c,c)}(\mathbf{r}_2, \mathbf{r}_3) \frac{4\pi}{q^2} \left(Z - \mathrm{e}^{\mathrm{i}\mathbf{q}\cdot\mathbf{r}_2} - \mathrm{e}^{\mathrm{i}\mathbf{q}\cdot\mathbf{r}_3}\right)\Phi_i(\mathbf{r}_2, \mathbf{r}_3), \tag{22}$$

while the matrix elements for $\mathbf{H}$ and $\mathbf{S}$ read:

$$\mathbf{H}_{\nu'',\nu'} = \int \mathrm{d}\mathbf{r}_2 \mathrm{d}\mathbf{r}_3\, \Theta_{\nu''}^{(c,c)}(\mathbf{r}_2, \mathbf{r}_3)\Big[-\beta_{n_2 l_2}\mathcal{V}^{(c)}(r_2) - \beta_{n_3 l_3}\mathcal{V}^{(c)}(r_3) + \frac{1}{r_{23}}\Big]\Theta_{\nu'}^{(c,c)}(\mathbf{r}_2, \mathbf{r}_3), \tag{23a}$$

$$\mathbf{S}_{\nu'',\nu'} = \int \mathrm{d}\mathbf{r}_2 \mathrm{d}\mathbf{r}_3\, \Theta_{\nu''}^{(c,c)}(\mathbf{r}_2, \mathbf{r}_3)\Theta_{\nu'}^{(c,c)}(\mathbf{r}_2, \mathbf{r}_3). \tag{23b}$$

Problem (11) is separable in eigenstates of the total angular momentum of electrons 2 and 3, and thus equation (21) is solved separately for each set of numbers $\{L', M'\}$.

Using the GSF tools we have solved equation (11) for energies corresponding to the Orsay experiment: the projectile has an incident energy of 5599 (5587) eV and each ejected electron has 10 (4) eV. The ionized electrons are detected in the plane determined by the incident and final momenta of the projectile, configuration known as in-plane. Projectiles scattered at a small angle are measured in that experiment: $\theta_s = 0.45°$. This leads to a small momentum transfer of 0.24 a.u. in the (10+10) eV case and 0.22 a.u. in the (4+4) eV case, angled respectively at 319° and 315° from the incident direction.

In figure 1 we show the real part of the scattering function for two partial waves in the (10+10) eV case. One clearly observes hyperspherical wave fronts (i.e., in the hyperradius $\rho = \sqrt{r_2^2 + r_3^2}$) as those described in equation (127) of [26]. Since the hyperspherical behaviour is not explicitly contained in the three-body GSF basis elements (equation (20)), the presence of those fronts proves that the electron–electron correlation is being correctly included in our calculations through the combination (19). Because of the presence of the helium bound state, the RHS of equation (11) is already numerically negligible for r_2 and r_3 values larger than 15 a.u. This means that, outside this small domain, all the effort done by the GSF basis is concentrated in expanding the electron–electron correlation and building the three-body Coulomb wave function corresponding to partial waves indexed by quantum numbers $\{L', M', l_2', l_3'\}$.

In section 2 we showed that the transition amplitude (15) for the ionization process can be extracted from the asymptotic behavior of the wave function. We worked with a partial wave expansion, and within such scheme, the hyperspherical wave fronts with Peterkop asymptotic conditions should be present on each partial wave, as studied by Kadyrov and collaborators [26]. In that reference, a quite intrincate expression for each asymptotic component is derived. Our solution numerically builds the correct behavior to be expected for the partial wave terms as illustrated in figure 1.

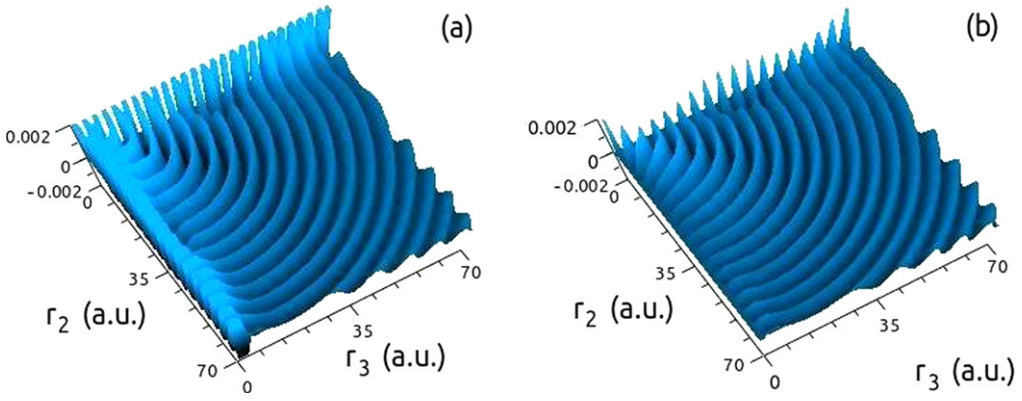

Figure 1. Sample partial waves (real part) of our calculations of the (e, $3e$) process on helium with the GSF method in the (10+10) eV kinematics reported in [16], as functions or r_2, r_3. (a) Partial wave corresponding to $L' = 1$, $l_2' = 0$, $l_3' = 1$. (b) Partial wave corresponding to $L' = 1$, $l_2' = 1$, $l_3' = 2$.

In the following section, we will present and analyze our resulting fivefold differential cross sections (FDCS):

$$\frac{\mathrm{d}^5\sigma}{\mathrm{d}\Omega_2\mathrm{d}\Omega_3\mathrm{d}\Omega_f\mathrm{d}E_2\mathrm{d}E_3} = (2\pi)^4\frac{k_f k_2 k_3}{k_i}\left|T_{\tilde{\mathbf{k}}_2,\tilde{\mathbf{k}}_3}\right|^2 \qquad (24a)$$

$$= (2\pi)^3\frac{k_f k_2 k_3}{k_i\kappa^3}\lim_{\rho\to\infty}\rho^5\left|\Phi_{sc}^{+}(\mathbf{q},\mathbf{r}_2,\mathbf{r}_3)\right|^2, \qquad (24b)$$

where the second equality derives from equation (14). What we actually do is to evaluate the scattering wave function at a finite, but sufficiently large, hyperradius ρ. It is important to stress that the wavefunction contains the information of all the energetically viable fragmentation channels. Throughout this work we study equal energy sharing, and therefore extract the transition matrix from $\alpha = \pi/4$.

4. Results

Our calculated FDCS are now presented for both kinematical sets ((10+10) eV and (4+4) eV) and compared with the Orsay absolute experimental data [16]. When possible, comparison is also made with two other *ab initio* calculations: the CCC ([16, 27]) and J-Matrix ([28], based on the same methods as [13, 14]). For all FDCS plots, the ejection angles are measured in degrees with respect to the projectile incident direction.

An important part of the numerical implementation is the convergence of the results with respect to the partial waves L' for the continuum solution. Knyr *et al* [14] found that it was sufficient to include up to $L' = 2$. We performed a test that confirmed their assertion: it consisted in comparing the magnitudes of the expansion coefficients $\phi_{\nu'}^{(c,c)}$ resulting from calculations with $L' = 0$, 1, 2, 3 and 4. After $L' = 2$ there is a drop off of two orders of magnitude in both the average and largest $\phi_{\nu'}^{(c,c)}$ for the given partial wave. Therefore, it can be considered as safe to work with total angular momentum up to 2, at least for the small momentum transfer regime under scrutiny.

We have performed calculations on different spatial domains ranging from 30 × 30 a.u. to 70 × 70 a.u. and always observed hyperspherical fronts as those shown in figure 1. The FDCS presented in this section were extracted from the scattering wavefunction at $\rho = 65$ a.u. (70 × 70 a.u. calculation) with a 10% relative confidence band for the extracted cross sections. The incidence of the ρ value has been discussed in [29], where we report no important difference between an extraction at $\rho = 48$ a.u. and $\rho = 68$ a.u.

4.1. (10+10) eV kinematics

We first provide, in figure 2, our GSF results generated with the Temkin–Poet model of the helium target. A good agreement in shape and magnitude with the experimental FDCS is observed, in particular in frames (b), (c) and (e). We stress that no renormalization whatsoever is needed here. A similar agreement (in both shape and magnitude) was reported in [30] by using simplified bound and continuum three-body wave functions. Under the light of further investigation [31, 32] this was shown to be fortuituous. Theoretical results arising from simplified models (with, for example, good asymptotic behaviour) may work, but a quantitative agreement with experiments is likely to be due to plain luck.

We now turn (and for the rest of the presentation) to the more advanced helium ground state expansion, including additional partial waves resulting in a bound energy of –2.90277 a.u. and -2.90334 a.u. In figures 3–7 we display the FDCS plots corresponding to the experimental geometries presented in [16]. Comparison is established with the J-Matrix theory for all cases, and with the CCC when available. Theoretical results are upscaled by multiplicative factors as indicated in the captions. The introduction of more inter-electronic correlation in the target bound state, makes our FDCS depart, in magnitude, from its agreement with the experimental counterpart, but reach a good proximity with that of the CCC theory. No critical variation was observed in the FDCS upon the addition of two helium target partial waves (i.e., from $l_2 = l_3 \leqslant 2$ to $l_2 = l_3 \leqslant 4$). This indicates that at least for the present energy and momentum transfer regimes, the helium ground state does not require higher

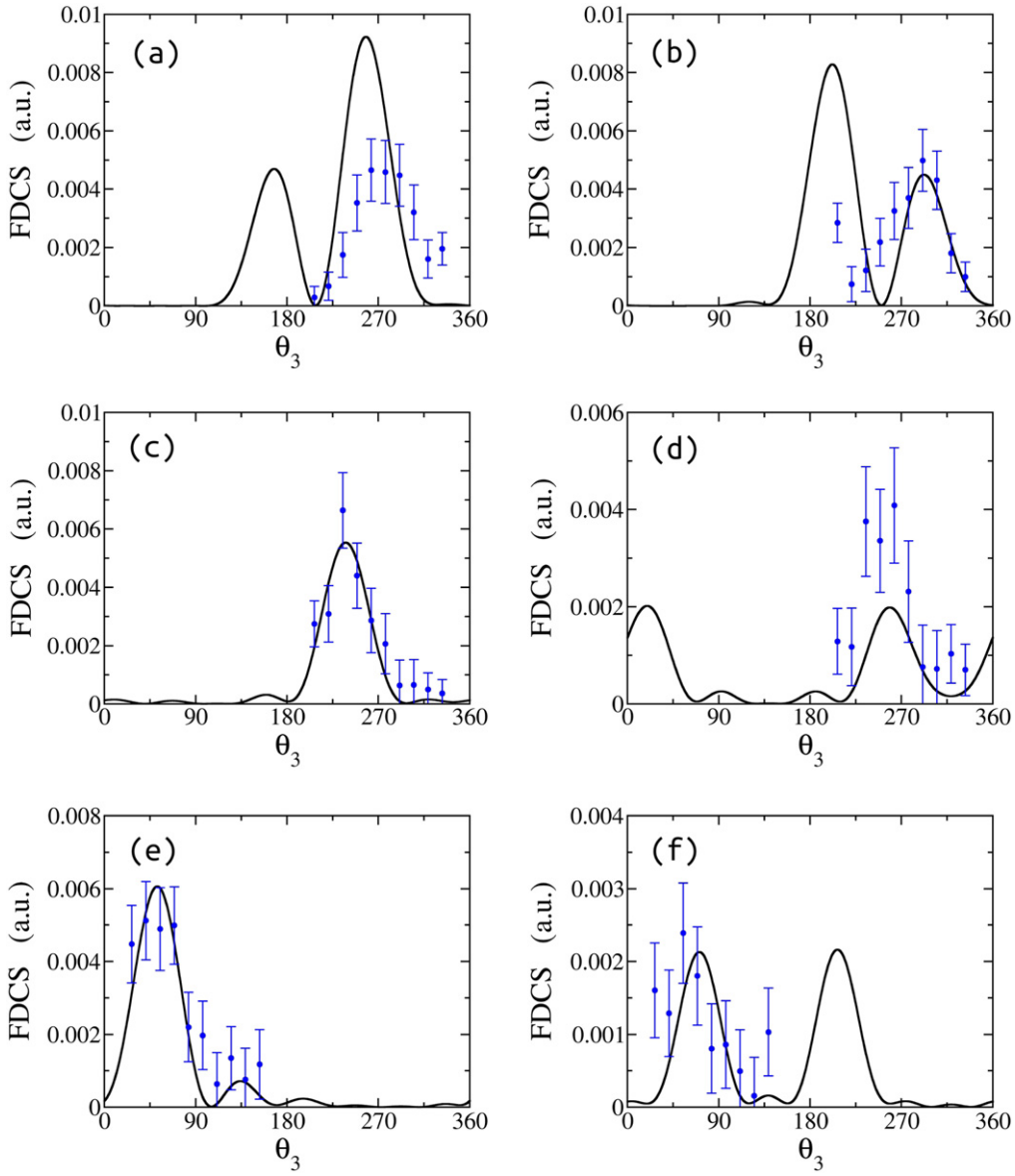

Figure 2. FDCS under the (10+10) eV kinematics as a function of ejection angle θ_3, with fixed angle at θ_2: (a) $\theta_2 = 27°$, (b) $\theta_2 = 69°$, (c) $\theta_2 = 111°$, (d) $\theta_2 = 139°$, (e) $\theta_2 = 291°$, (f) $\theta_2 = 319°$. The circles correspond to experimental data with error bars from [16]. Solid line: our GSF result, without renormalization, obtained with a Temkin–Poet helium ground state.

precision. Thus, a better agreement with the experiments is not to be expected by further improving the description of the target. For first Born order calculations, there is a symmetry to be expected in the FDCS when one of the electrons is emitted parallel or antiparallel to **q**: this is indeed the case as seen, respectively, in figures 5(i) and 7(s).

A further comparison is made with the CCC method in contour plots of the FDCS as a function of the ejection angles of both electrons, θ_2 and θ_3 (figure 8). It is worth mentioning that both methods present a similar minima structure, which is inherited from the small q regime. The peaks (recoil and binary) are slightly wider in the GSF case, but the magnitude is essentially the same, as is the physics contained in the results. It also can be asserted that the electron ejection velocities are predominantly orthogonal to each other. This seems to describe a classical collision between equal mass particles, one of them having initially a much smaller velocity. Any first order treatment considers a single collision of the projectile with strictly one particle of the target. Subsequently, the three interacting bodies redistribute the energy and momentum; this is modelled to all orders in our *ab initio* calculation. With that informaton we can establish which of the collision processes listed in the review by Berakdar *et al* [10] play a major role in this regime. The three processes pictorially represented in figure 9 imply a single collision between the two Helium electrons, right after one of them took the momentum transferred from the projectile. The subsequent impact renders both target electrons with nearly orthogonal velocities. Process (a) is commonly named *Two–Step–1*. Processes (b) and (c) correspond to one additional order in the multiple scattering scheme of [10] due to an extra

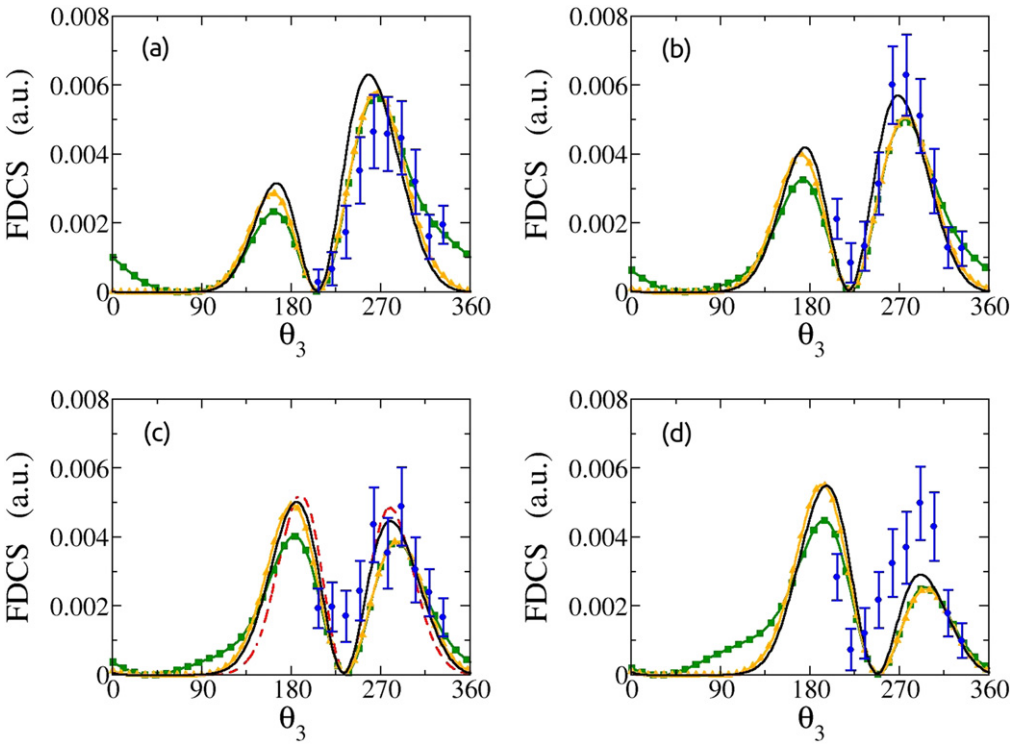

Figure 3. FDCS for the (10+10) eV kinematic condition plotted for ejection angle θ_3, with fixed θ_2 at: (a) $\theta_2 = 27°$, (b) $\theta_2 = 41°$, (c) $\theta_2 = 55°$, (d) $\theta_2 = 69°$. GSF upscaled by a factor 2.2 (helium ground state up to $l_2 = l_3 = 2$: orange line with triangles ; helium ground state up to $l_2 = l_3 = 4$: black continuous line); CCC [8] upscaled also by 2.2 (where available, red dashed line); J-Matrix ([28], based on the methods presented in [14]) upscaled by 1.2 (green continuous line with squares). Experimental data is from [16] (blue dots with error bars).

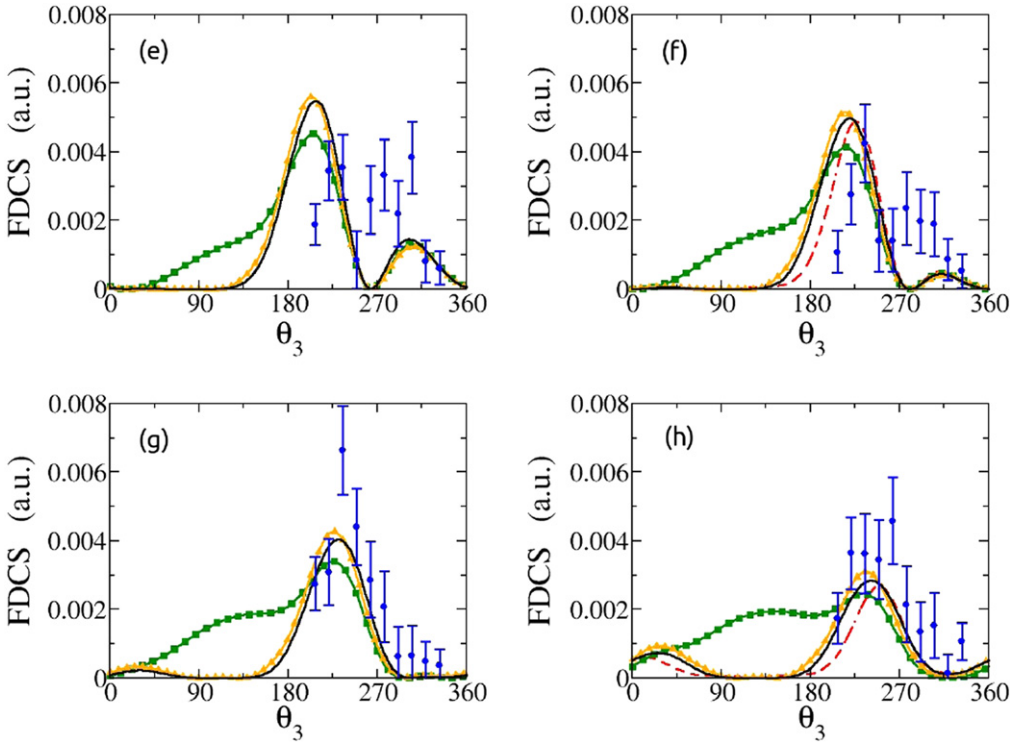

Figure 4. Same as figure 3, but for fixed ejection angles θ_2: (e) $\theta_2 = 83°$, (f) $\theta_2 = 97°$, (g) $\theta_2 = 111°$, (h) $\theta_2 = 125°$.

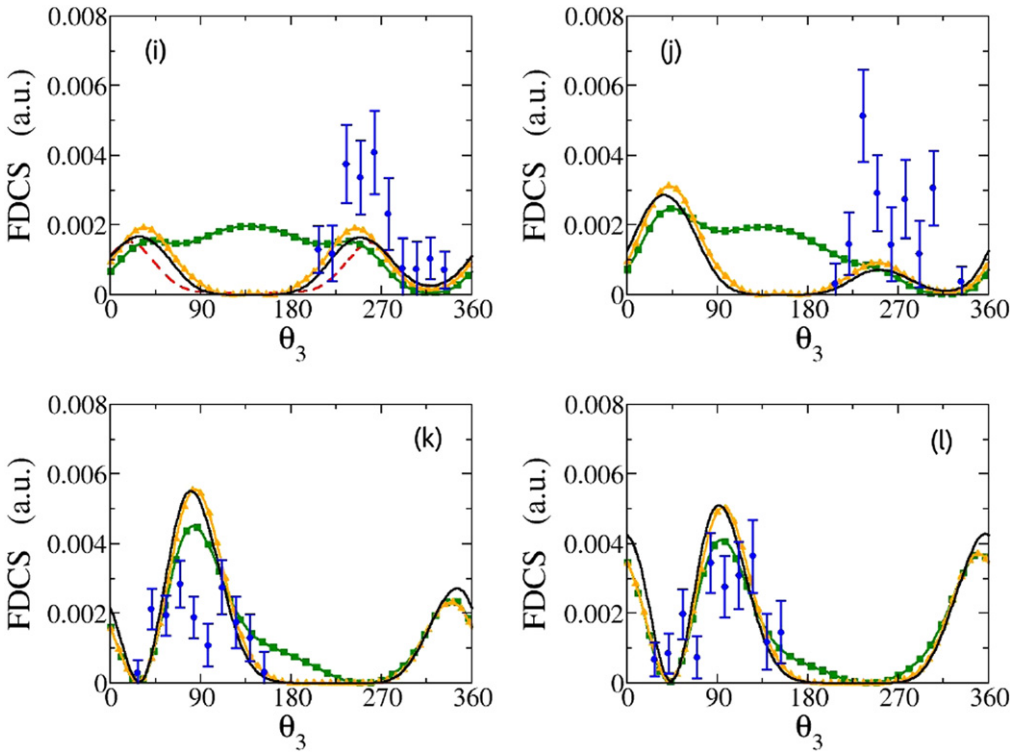

Figure 5. Same as figure 3, but for fixed ejection angles θ_2: (i) $\theta_2 = 139°$, (j) $\theta_2 = 153°$, (k) $\theta_2 = 207°$, (l) $\theta_2 = 221°$.

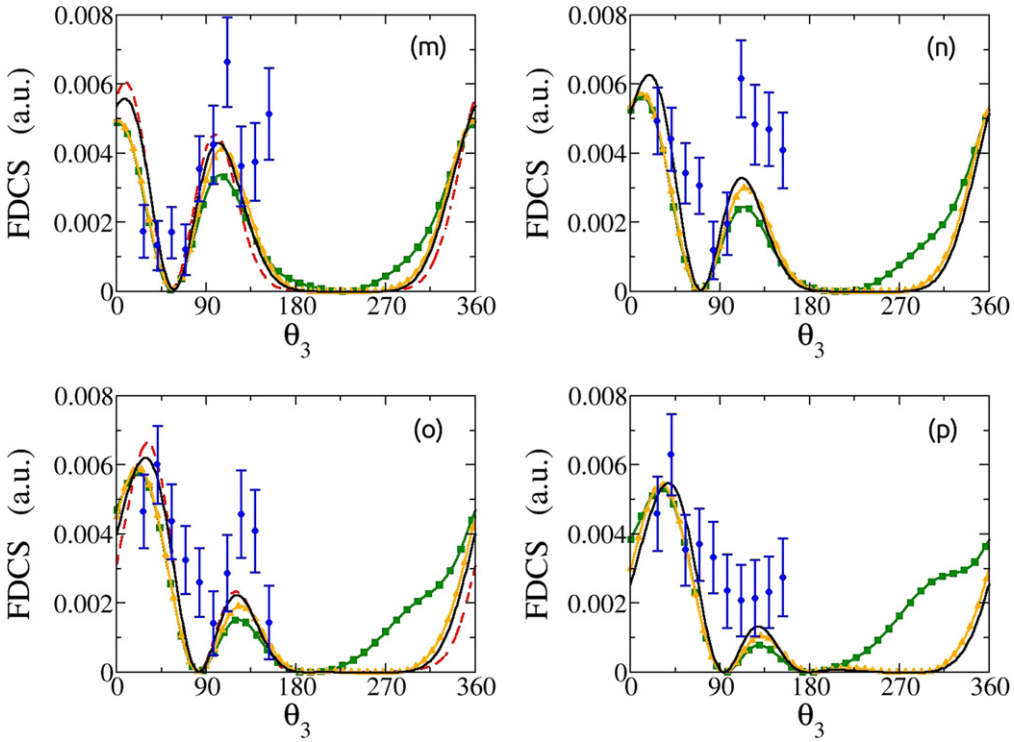

Figure 6. Same as figure 3, but for fixed ejection angles θ_2: (m) $\theta_2 = 235°$, (n) $\theta_2 = 249°$, (o) $\theta_2 = 263°$, (p) $\theta_2 = 277°$.

impact. Their contribution is expected to be somewhat smaller, yet naturally contained in our First Born calculation.

In figure 10 we present a zoomed-in version of figure 8 where the scale has been set to reach its maximum at 0.0003 a.u., with the purpose of observing phenomena that would be shadowed by comparison with the main structures, namely the recoil (R) and binary (B) peaks. The red circles denote the condition where there is a minimum momentum transfer to the ion, approaching the Bethe sphere behaviour [18, 24]. Figure 11 supplements this argument, showing the magnitude

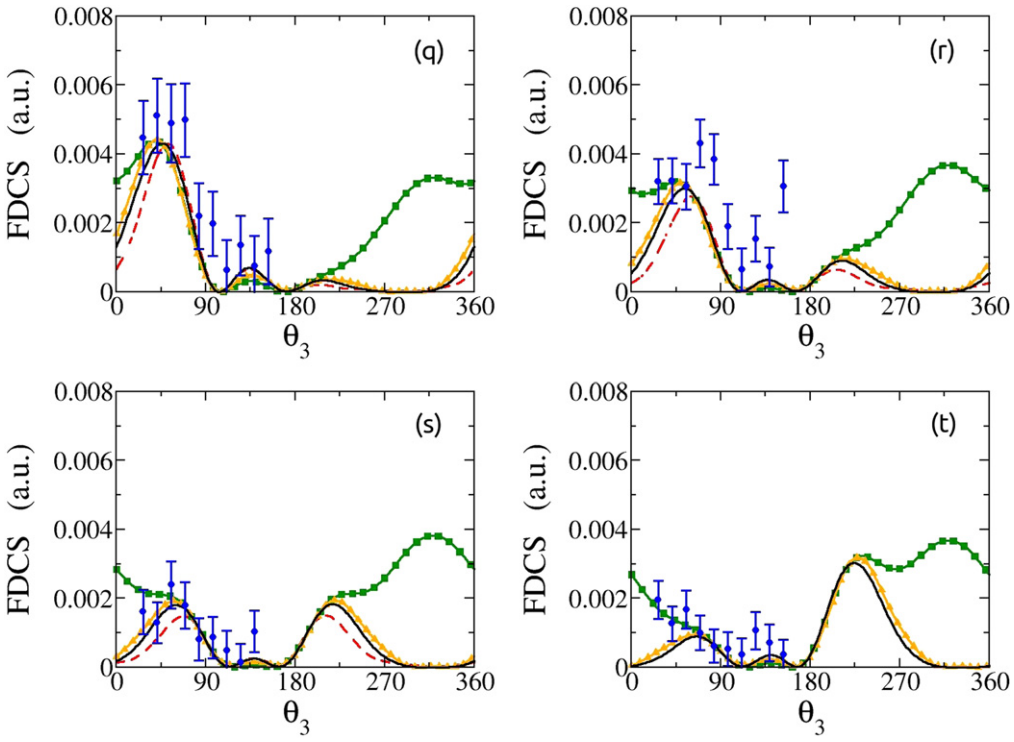

Figure 7. Same as figure 3, but for fixed ejection angles θ_2: (q) $\theta_2 = 291°$, (r) $\theta_2 = 305°$, (s) $\theta_2 = 319°$, (t) $\theta_2 = 333°$.

of the momentum transferred to the resulting He^{++} ion for different θ_2 and θ_3. The Bethe sphere is reached when the ejected electrons emerge in roughly back-to-back configuration. This, in turn, is strongly suppressed under the dipolar regime, and the two phenomena compete with each other, the result being the little humps observed in figures 5(i) and 7(s).

Figure 10 also shows the minimal FDCS lines which would correspond to strict zeros in the photoionization limit (i.e., $q \to 0$) of this problem. The (red) squares denote the minima to be expected due to both electrons being emitted with momenta verifying $\mathbf{k}_2 \cdot \mathbf{q} = 0 = \mathbf{k}_3 \cdot \mathbf{q}$. Within the in-plane geometry those minima are coincident with the minima due to back–to–back emission ($\mathbf{k}_2 = -\mathbf{k}_3$), colinear emission ($\mathbf{k}_2 = \mathbf{k}_3$) and with $\left(\mathbf{k}_2 + \mathbf{k}_3\right) \cdot \mathbf{q} = 0$, configurations analyzed in detail by Lahmam–Bennani *et al* in [18].

4.2. (4+4) eV kinematics

The agreement between the GSF and the CCC theories is even more remarkable under this kinematic condition. We show in figure 12 the comparison between these theories, both rescaled up by a factor of 14 to match the experimental data. We present in figure 12 FDCS for two key θ_2 configurations, namely, at right angles with $\mathbf{q}$ ($\theta_2 = 45°$ and $\theta_2 = 225°$). The parallel and antiparallel configurations have already been shown to present agreement with the CCC in [29]. Both panels in figure 12 show a slight difference in the height of the peaks is observed between GSF and CCC calculations. The GSF results seem to be more physically plausible: the recoil and binary structures need not be of equal height, since the parallel and antiparallel directions are not physically equivalent [33].

In figures 13 and 14 the interest is shifted towards the comparison of both theoretical *ab initio* schemes: the GSF and the CCC show remarkable agreement between them, both in shape and magnitude. We present in those figures FDCS—without renormalizing either theory—for several other θ_2 configurations.

Finally, contour plots for the FDCS for the (4+4) eV kinematics are presented in figure 15 where the agreement between the CCC and GSF results is clearly observable, and is even more pronounced than that presented in figure 8 for the (10+10) eV case.

5. Concluding remarks

Motivated by the still standing controversy on the fast electron impact double ionization of Helium, we applied the GSF method to study this process employing the kinematical conditions of the Orsay (e, $3e$) coplanar experiment. Those data sets possess a useful, rarely available feature: to be on an absolute scale. This in principle should be useful to discriminate between theories predicting similar qualitative FDCS shapes, but different magnitudes.

A simplified set of calculations, using a Temkin–Poet helium target, yielded surprising agreement with the experimental data without the need for a renormalization. Usage of simpler models can sometimes lead to fortuitously good agreement with the experiments, as was the case in [30].

When other partial waves were added to the helium target, the agreement in magnitude with the experimental set vanished, but a fairly good agreement with the CCC

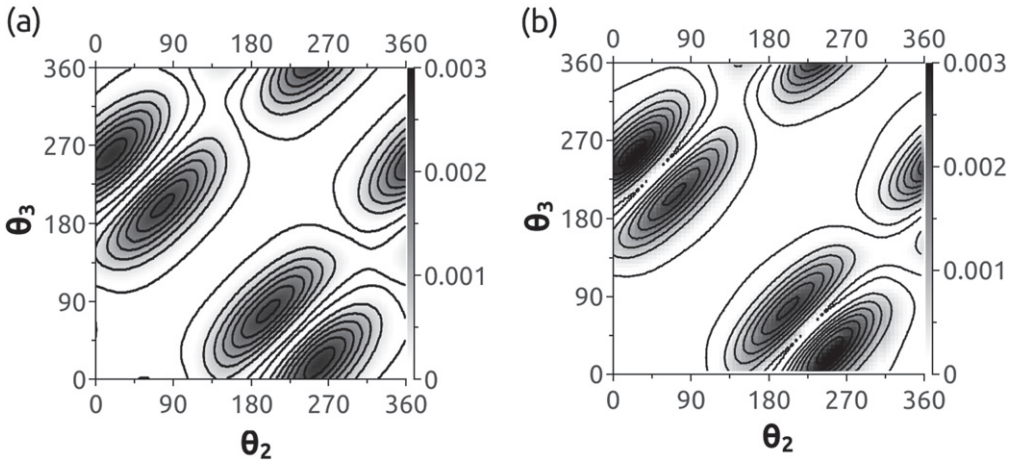

Figure 8. Contour plots for FDCS as a function of the ejection angles θ_2 and θ_3 under the (10+10) eV kinematics: GSF (a) vs CCC (b). The interest is shifted towards a theoretical result comparison, and thus no rescaling is applied to either set.

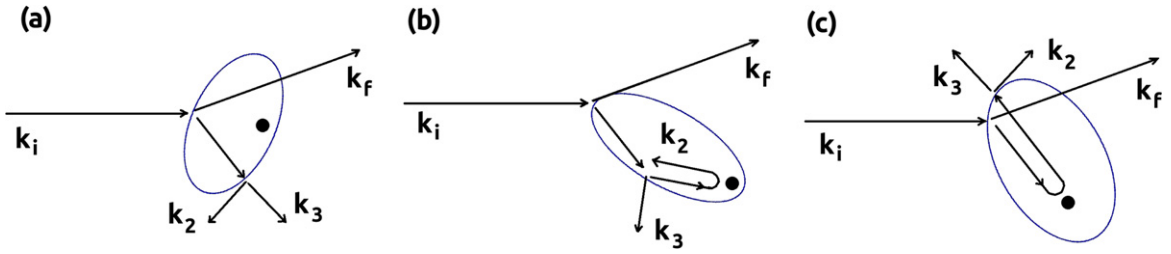

Figure 9. Dominant processes evidenced by the FDCS presented in figure 8.

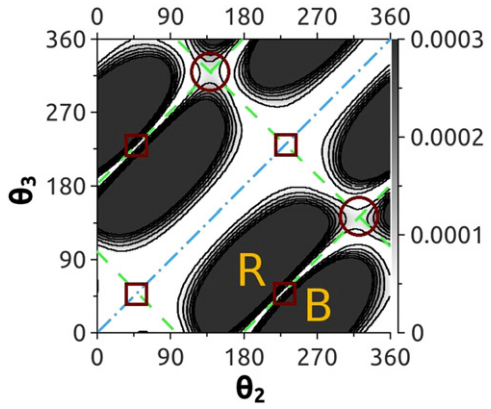

Figure 10. FDCS obtained with the GSF method. The scale has been chosen to have a saturation value of 0.0003, in order to perceive details that would be hidden with a scale commesurate with the recoil and binary peaks. The minima structure due to interelectronic repulsion is plotted in dash–dot line. In dashed lines with positive slope: the minima for back-to-back emission. The dashed lines with negative slope correspond to the case $(\mathbf{k}_2 + \mathbf{k}_3) \cdot \mathbf{q} = 0$. With the red squares we point to configurations which imply $\mathbf{k}_2 \cdot \mathbf{q} = 0$ and $\mathbf{k}_3 \cdot \mathbf{q} = 0$ simultaneously. The red cirles denote configurations where there is a maximal momentum transfer to the electrons.

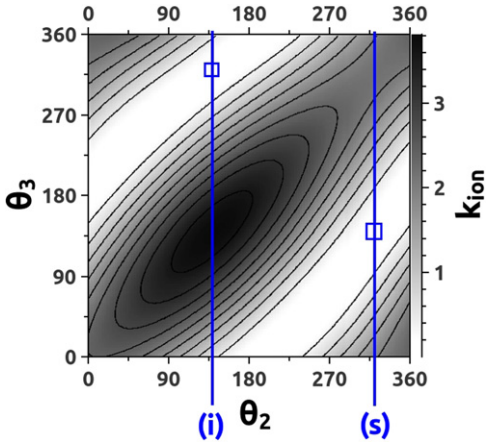

Figure 11. Magnitude of the momentum tranferred to the He^{++} ion as a function of the emission angles of the electrons in the (10+10) eV case. The marked vertical lines indicate the $\theta_2 = 139°$ and $\theta_2 = 319°$ cuts, through which the FDCS is plotted in figures 5(i) and 7(s). The squares correspond to the circles marked in figure 10, which are minima of the momentum transferred to the nucleus.

theory emerged. Even more impressive than the one found for the (10+10) eV set was the agreement obtained for the (4+4) eV kinematics. We observed no appreciable change in the FDCS with further addition of helium target partial waves.

The agreement with the CCC theory under both kinematic conditions is better than any previously reported [12]. Having two different theories agreeing in the FDCS, not just in shape but also in magnitude, leads us to believe that the problem is correctly solved at least in the fast projectile and quasi–photon regimes. Consequently, two main lines of reasoning emerge. The first one is that the experiments could have had some kind of systematic error leading to an

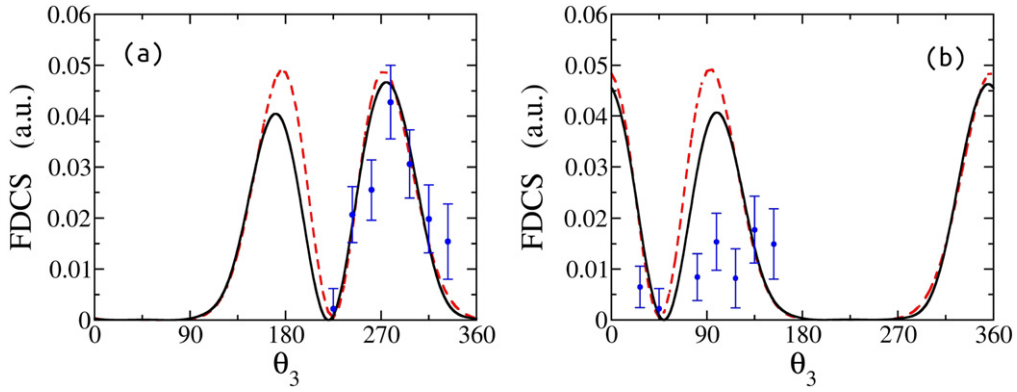

Figure 12. FDCS for the (4+4) eV kinematic condition plotted for ejection angle θ_3, with fixed θ_2 at: (a) $\theta_2 = 45°$, (b) $\theta_2 = 225°$, GSF (black continuous line), CCC [16] (red dashed line), experimental results (blue dots with error bars) from [16]. All calculations renormalized to compare with the experiments, up by the same factor 14.

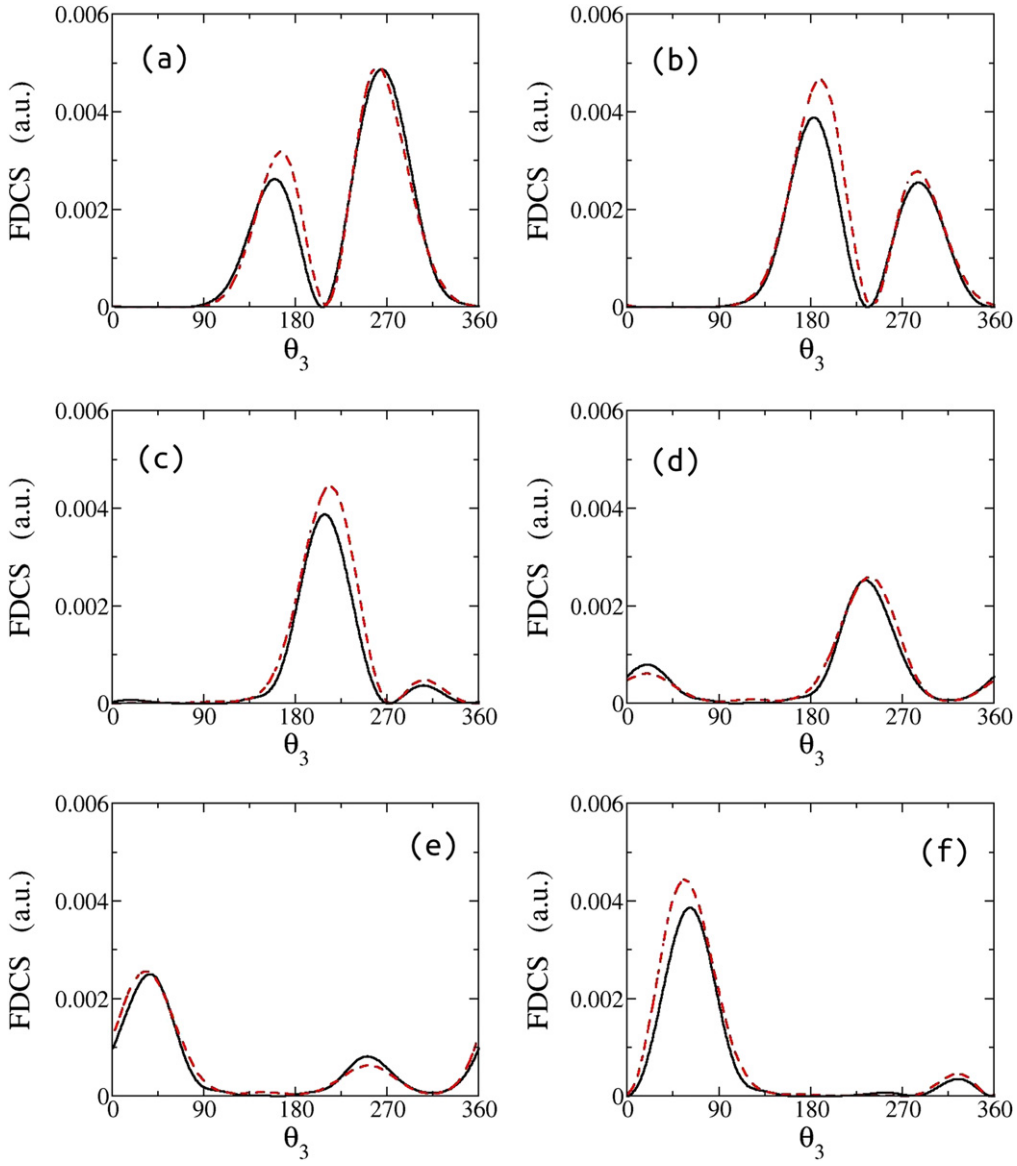

Figure 13. FDCS for the (4+4) eV kinematic condition plotted for ejection angle θ_3, with fixed θ_2 at: (a) $\theta_2 = 30°$, (b) $\theta_2 = 60°$, (c) $\theta_2 = 90°$, (d) $\theta_2 = 120°$, (e) $\theta_2 = 150°$, (f) $\theta_2 = 180°$. GSF (black continuous line) and CCC ([34] with the same methods as in [16]) (red dashed line), not rescaled.

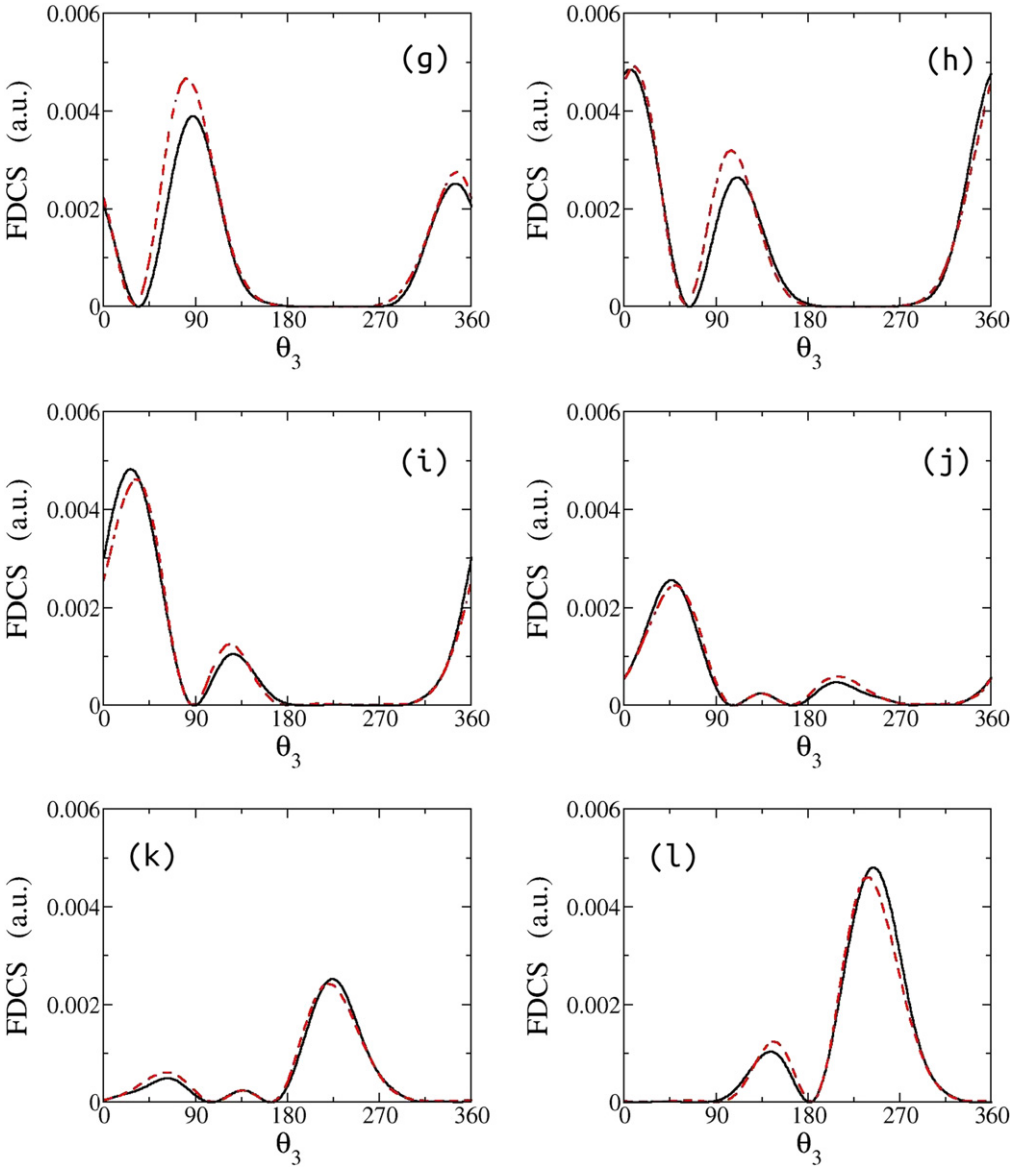

Figure 14. Same as figure 13 but with θ_2 fixed at: (g) $\theta_2 = 210°$, (h) $\theta_2 = 240°$, (i) $\theta_2 = 270°$, (j) $\theta_2 = 300°$, (k) $\theta_2 = 330°$, (l) $\theta_2 = 360°$.

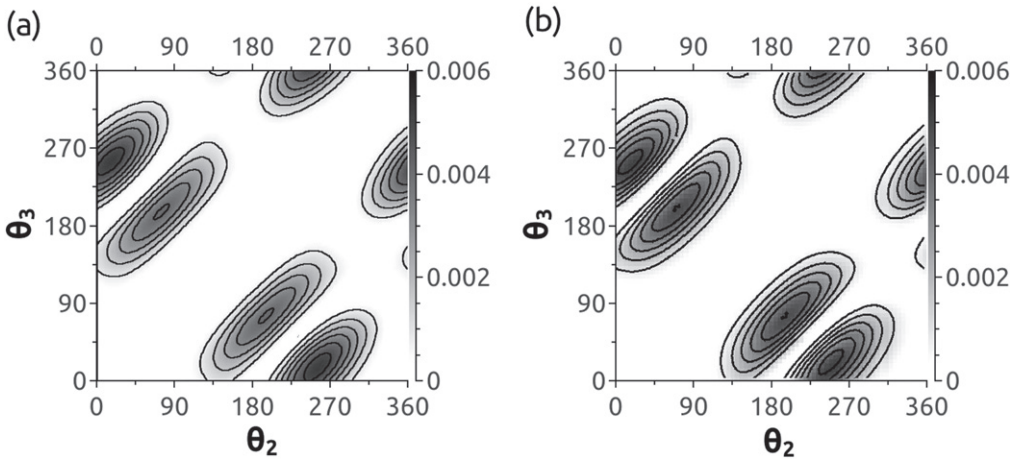

Figure 15. Contour plots for FDCS as a function of the ejection angles θ_2 and θ_3 under the (4+4) eV kinematics: GSF (a) vs CCC (b). No rescaling is applied to either set.

overestimation of the FDCS, particularly severe for the (4+4) eV case. More so, the experimental data does not conform with the expected minima for all emission geometries under the small momentum transfer regime. However, since experiments in principle hold a stronger footing than theoretical calculations, one is led to the second line of reasoning. Could it be possible then, for the theoretical First Born model, which by now we know is correctly solved, to be leaving out some essential interaction mechanism? For instance, it was already stated that the fast projectile model considers only a single deflection of the projectile. This consideration has worked fine for the ionization of the hydrogen atom by fast electrons. However, since the helium target contains an additional electron, could processes involving two deflections of the projectile be playing a not-so-negligible role? Kheifets' work [35] can be considered a prospective lookout on the second Born order. In that work the author concludes that the second order corrections only change the FDCS very weakly at ≈5.6 keV incident energy. This is also backed by other approaches involving asymptotically correct (yet approximate) functions for the initial and final states of the system [36, 37]. Pointing in the opposite direction are the results presented by Berakdar [38], which suggest that interference between different terms of the Green operator expansion generates a more rapidly varying structure for the FDCS not present in FBA calculations [13–16]. However, this argument cannot be claimed to be conclusive, since Berakdar's calculations were performed with approximate, asymptotically correct, solutions. To completely close the discussions on this topic, more in-depth theoretical studies are necessary on the second Born approximation, as well as more experimental sets with absolute scale.

Acknowledgments

We want to thank Dr Anatoly Kheifets, Dr Sergei Zaytsev and Prof. Lahmam–Bennani for providing FDCS results in tabular form. This work has been developed within the activities planned in the French-Argentinian program ECOS-Sud A10E01. We acknowledge the CNRS (PICS project No. 06304) and CONICET (project No. Dl 158114) for funding our French-Argentinian collaboration. The support by ANPCyT (PICT08/0934) (Argentina) and PIP 200901/552 CONICET (Argentina) is acknowledged. GG also thanks the support by PGI (24/F059) of the Universidad Nacional del Sur.

References

[1] Lopez X, Ugalde J, Echevarría L and Ludeña E 2006 *Phys. Rev.* A **74** 042504
[2] Loos P F 2010 *Phys. Rev.* A **81** 032510
[3] Otranto S and Olson R E 2008 *Phys. Rev.* A **77** 022709
[4] Bray I 2002 *Phys. Rev. Lett.* **89** 273201
[5] Rescigno T N, Baertschy M, Isaacs W A and McCurdy C W 1999 *Science* **286** 2474
[6] Malegat L, Selles P and Kazansky A 2000 *Phys. Rev. Lett.* **85** 4450
[7] McCurdy C W and Martín F 2004 *J. Phys. B: At. Mol. Opt. Phys.* **37** 917
[8] Kheifets A S and Bray I 2004 *Phys. Rev.* A **69** 050701(R)
[9] Bray I, Fursa D V, Kadyrov A S, Stelbovics A T, Kheifets A S and Mukhamedzhanov A M 2012 *Phys. Rep.* **520** 135–74
[10] Berakdar J, Lahmam-Bennani A and Dal Cappello C 2003 *Phys. Rep.* **374** 91
[11] Gasaneo G, Mitnik D M, Randazzo J M, Ancarani L U and Colavecchia F D 2013 *Phys. Rev.* A **87** 042707
[12] Ancarani L U, Cappello C D and Gasaneo G 2010 *J. Phys.: Conf. Ser.* **212** 012025
[13] Knyr V A, Nasyrov V V and Popov Y V 2003 *AIP Conf. Proc.* **697** 76
[14] Alhaidari A D, Heller E J, Yamani H A and Abdelmonem M S 2008 *The J-matrix Method: Developments and Applications* (Dordrecht: Springer) pp 137–143
[15] Silenou Mengoue M, Kwato Njock M G, Piraux B, Popov Y V and Zaytsev S A 2011 *Phys. Rev.* A **83** 052708
[16] Kheifets A, Bray I, Bennani L, Duguet A and Taouil I 1999 *J. Phys. B: At. Mol. Opt. Phys.* **32** 5047
[17] Serov V, Derbov V, Joulakian B and Vinitsky S 2007 *Phys. Rev.* A **75** 012715
[18] Lahmam-Bennani A, Taouil I, Duguet A, Lecas M, Avaldi L and Berakdar J 1999 *Phys. Rev.* A **59** 3548
[19] Ambrosio M J, Gasaneo G and Colavecchia F D 2014 *Phys. Rev.* A **89** 012713
[20] Gasaneo G, Ancarani L U, Mitnik D M, Randazzo J M, Frapiccini A L and Colavecchia F D 2013 *Adv. Quantum Chem.* **67** 153–216
[21] Ambrosio M J, Ancarani L U, Mitnik D M, Colavecchia F D and Gasaneo G 2014 *Few-Body Syst.* **55** 825–9
[22] Kadyrov A S, Mukhamedzhanov A M, Stelbovics A T, Bray I and Pirlepesov F 2003 *Phys. Rev.* A **68** 022703
[23] Alt E O and Mukhamedzhanov A M 1993 *Phys. Rev.* A **47** 2004
[24] Berakdar J and Klar H 1994 *J. Phys. B: At. Mol. Opt. Phys.* **26** 4219
[25] Mitnik D M, Colavecchia F D, Gasaneo G and Randazzo J M 2011 *Comput. Phys. Commun.* **182** 1145
[26] Kadyrov A S, Mukhamedzhanov A M, Stelbovics A T and Bray I 2004 *Phys. Rev.* A **70** 062703
[27] Kheifets A S, Bray I, Berakdar J and Cappello C Dal 2002 *J. Phys. B: At. Mol. Opt. Phys.* **35** L15
[28] Zaytsev S 2013 private communication
[29] Ambrosio M J, Colavecchia F D, Mitnik D M and Gasaneo G 2015 *Phys. Rev.* A **91** 012704
[30] Jones S and Madison D H 2003 *Phys. Rev. Lett.* **91** 073201
[31] Ancarani L U, Montagnese T and Dal Cappello C 2004 *Phys. Rev.* A **70** 012711
[32] Ancarani L and Dal Cappello C 2007 *J. Electron Spectrosc. Relat. Phenom.* **161** 22
[33] Dorn A, Kheifets A, Schröter C, Najjari B, Höhr C, Moshammer R and Ullrich J 2002 *Phys. Rev. Lett.* **65** 032709
[34] Kheifets A 2014 private communication
[35] Kheifets A S 2004 *Phys. Rev.* A **69** 032712
[36] Grin M, Cappello C D, Mkhanter R E and Rasch J 2000 *J. Phys. B: At. Mol. Opt. Phys.* **33** 131
[37] Ancarani L U, Montagnese T and Dal Cappello C 2005 Electron and photon impact ionization and related topics *IOP Conf. Proc.* ed B Piraux (London: Institute of Physics Publishing) p 21
[38] Berakdar J 2000 *Phys. Rev. Lett.* **85** 4036